Quaternary Research (2018), **89**, 270–280.

doi:10.1017/qua.2017.81

A lacustrine record of East Asian summer monsoon and atmospheric dust loading since the last interglaciation from Lake Xingkai, northeast China

Weiwei Sun[a]*, Ji Shen[a]*, Shi-Yong Yu[b], Hao Long[a], Enlou Zhang[a], Enfeng Liu[c], Rong Chen[a]

[a]State Key Laboratory of Lake Science and Environment, Nanjing Institute of Geography and Limnology, Chinese Academy of Sciences, Nanjing 210008, China
[b]School of Geography, Geomatics, and Planning, Jiangsu Normal University, Xuzhou 221116, China
[c]College of Geography and Environment, Shandong Normal University, Jinan 250014, China

(Received November 10, 2016; Accepted August 15, 2017)

Abstract

A 336-cm-long sediment core spanning the last 130 ka was recovered from Lake Xingkai on the northeastern margin of the East Asian summer monsoon domain to reveal the linkage between lacustrine depositional processes and environmental changes. Bayesian end member modeling analysis was conducted to partition and interpret the grain-size distributions of Lake Xingkai sediments. Our results suggest that the sedimentary system is characterized by three end members (EMs). EM1 and EM2, with a modal value of 13 and 10 μm, respectively, indicate the variation of local hydraulic conditions. EM3, with a modal value of 5 μm, reflects the background atmospheric dust loading. High atmospheric dust concentration generally occurred during Marine Isotope Stage (MIS) 5d, MIS 4, and early MIS 3, when the climate in the Asian dust source region was cold and dry. In contrast, low dust concentration prevailed during MIS 2, likely due to the southward shift of the westerlies driven by maximum ice volume in the high latitudes.

Keywords: Asian summer monsoon; Dust loading; Westerlies; Grain-size; End member analysis; Lake Xingkai

INTRODUCTION

Located on the margin of the East Asian summer monsoon (EASM) domain, the arid and semiarid zones in north China and Mongolia are particularly sensitive to climate change. Prolonged droughts in these areas caused by the weakened EASM could result in crop failure, soil degradation, and even desertification, posing detrimental impacts on human livelihood and ecosystem functionality (Lu et al., 2013; Yin et al., 2016). Specifically, the northern and western parts of East Asia represent an important dust source, where dust can be lifted and transported for thousands of kilometers by the westerlies to Korea, Japan, north Pacific Ocean, and even as far as North America (Uno et al., 2009). Dust aerosols are considered to play an important role in the climate system, influencing the Earth's radiative balance, marine biogeochemical cycle, and atmospheric chemical composition (Uno et al., 2009; Maher et al., 2010; Middleton and Sternberg, 2013). Many kinds of archives such as ice cores, loess-paleosol sequences, and marine sediment cores show that the average dust deposition rate was higher during glacials than that during interglacials (Rea and Hovan, 1995; Steffensen, 1997; Nagashima et al., 2007). However, the existing dust records appear to be latitudinally asynchronous, probably modulated by the meridional shift of the westerlies (Nagashima et al., 2007; Kang et al., 2015). Therefore, the relative contributions of source area aridity over the atmospheric circulations to the variations in the atmospheric dust loading inferred from geologic archives remain a topic of debate.

Lacustrine sediment grain-size parameters have been widely used to infer past environmental and climatic changes in various geological settings, as they are closely related to changes in provenance, transporting energy, and sedimentary process (Sun et al., 2002; Xiao et al., 2008; Dietze et al., 2012). For example, a few studies suggest that lacustrine deposits are often derived from multiple sediment sources, which are transported by different processes (e.g., fluvial, alluvial, aeolian, or glacial) and are well-mixed after being deposited in the lake basin (Liu et al., 2009; Dietze et al., 2012; Xiao et al., 2012; Xiao et al., 2013). Therefore, traditional approaches

*Corresponding authors at: State Key Laboratory of Lake Science and Environment, Nanjing Institute of Geography and Limnology, Chinese Academy of Sciences, Nanjing 210008, China. E-mail addresses: wwsun@niglas.ac.cn (W. Sun), jishen@niglas.ac.cn (J. Shen).

(e.g., moment-based descriptive statistics) are limited in scope and unable to unravel the complex transport and deposition processes from the spectrum of individual lacustrine sediment samples. Recently, many numerical methods, including curve fitting and eigenspace analysis, have been proposed to partition the grain-size components of sediments and retrieve proxy information sensitive to transport and deposition dynamics. Curve fitting using a prescribed kernel distribution function (e.g., lognormal or Weibull distribution function) requires some prior assumption of the grain-size distribution of the sub-population, resulting in the interpretation of the fitting parameters might be not be geologically meaningful (Yu et al., 2016). In contrast, eigenspace analysis makes full use of all samples based on principles of numerical inversion to reduce information redundancy and takes into account the unit-sum constraints. In this case, the shapes of the end members do not have to be specified (Dietze et al., 2012). Thus, eigenspace analysis should be particularly well-suited to the unmixing of grain-size distributions.

Lake Xingkai is the largest freshwater lake in northeast Asia and the climate is controlled by the interaction of the EASM and the westerlies systems. It is the only site chosen in northeast Asia for lake drilling in the Past Global Changes (PAGES) Pole-Equator-Pole program due to its critical location (Williams et al., 2001). During the past decade, the paleoenvironment and lake evolution have been reconstructed based on multi-proxy data from Lake Xingkai sediments and the formation of the surrounding sandy ridges (Wu and Shen, 2009, 2010a, 2010b; Zhu et al., 2011; Long and Shen, 2017). However, the 30 ka sedimentary record is at, or just over, the limits of obtaining reliable radiocarbon ages. Accelerator mass spectrometry (AMS) ^{14}C dates have been verified by an optically stimulated luminescence (OSL) dating study of Lake Xingkai sediments (Pigati et al., 2007; Long et al., 2015). In addition, the patterns of paleoclimate inferred from the surrounding sandy ridges are inconsistent (Zhu et al., 2011; Long and Shen, 2017).

In this study, we apply the Bayesian end-member-modeling analysis (BEMMA) proposed recently by Yu et al. (2016) to decompose the measured grain-size distributions into an optimal set of end members from Lake Xingkai in northeast China. The aim of the study was to interpret the environmental implications of the grain-size distributions of lacustrine deposits and reveal their links with changes in the EASM and the westerlies since the last interglaciation.

STUDY SITE

Lake Xingkai (44°32′–45°21′N, 131°58′–132°51′E, 65 m above sea level) is located on the border between China and Russia (Fig. 1a). Currently, the lake has a surface area of 4190 km^2 with a catchment area of 16,890 km^2. The lake is relatively shallow with a mean water depth of 4.5 m and a maximum water depth of 10 m. The lake is fed by five major rivers, including the Komissarovka, Mel'gunovka, Ilistaya, and Spasovka Rivers in Russia and the Baileng River in China, and it has only one outflowing river (the Songacha River), which flows into the Ussuri River (Fig. 1b). The lake basin is formed in a Cenozoic tectonic depression, which is filled by 200 m of Quaternary sediments (Wan and Zhong, 1997). Additionally, there are four sandy ridges ranging in width from 30 to 200 m located on the north side of Lake Xingkai in concentric arcs parallel with the lake present shoreline, known as Dahu, Taiyang, Er'dao, and Huang-Nan ridges in sequence from the lakeside. These are closely related to the lake evolution process (Long and Shen, 2017).

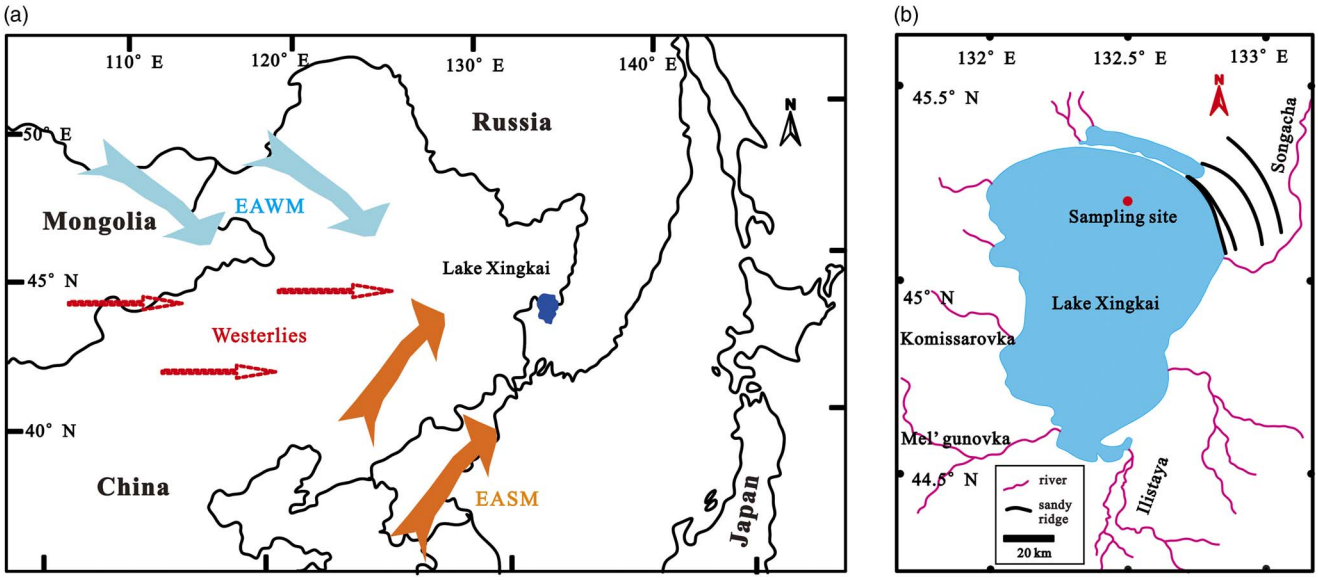

Figure 1. (a) Map showing the location of Lake Xingkai in northeast Asia (blue dot) and the dominant atmospheric circulation systems of East Asia (EASM, East Asian summer monsoon; EAWM, East Asian winter monsoon). (b) Map showing the catchment of Lake Xingkai and the drilling site (red dot). (For interpretation of the references to color inn this figure legend, the reader is referred to the web version of this article.)

https://doi.org/10.1017/qua.2017.81 Published online by Cambridge University Press

The climate of Lake Xingkai has a distinct seasonality in both temperature and precipitation (Shen, 2013; Wang et al., 2014; Long et al., 2015). In the summer, warm and humid air masses are transported by southwesterly winds from the western tropical Pacific; while in the winter, the climate is affected by the extremely dry and cold northwesterly winter monsoon caused by the Mongolia-Siberian High. Instrumental data available from the adjacent Jixi meteorological station (~120 km east of Lake Xingkai) indicate a mean annual temperature of 3°C with a maximum monthly mean temperature of 21°C in July and a minimum monthly mean of temperature −18°C in January. Mean annual precipitation is ~540 mm, around 70% of which falls between June and September. From late October to April, Lake Xingkai is covered by ice.

MATERIAL AND METHODS

In summer 2008, two parallel and overlapping sediment cores (XK08-A1 and XK08-A2) were collected from a water depth of 7 m near the China-Russia boundary (Fig.1b; 45°12'21"N, 132°30'33"E) using a UWITEC piston corer. In the laboratory, core correlation between XK08-A1 (308 cm long) and XK08-A2 (336 cm long) was carried out using surface scanning magnetic susceptibility as well as core XK-1 retrieved previously from the same site in summer 2007 (Wu and Shen, 2009) as a reference. Subsequently, core XK08-A1 was split under subdued red light in a dark room and sectioned at 5–10 cm intervals for optically stimulated luminescence (OSL) dating. A total of 49 OSL samples were obtained (Long et al., 2015). Core XK08-A2 was split into two halves and visually described in the field. The cores are mainly composed of fine-grained, grayish, minerogenic, organic-poor sediments. Coarse sands appear at 251–255 cm deep in Core XK08-A2. The working half of Core XK08-A2 was sectioned at 1 cm intervals, and the samples were stored at 4°C in the repository prior to analysis.

Because radiocarbon dating using the AMS method might be problematic for samples older than 30 cal ka BP, the chronology of cores XK08-A2 and XK-1 is mainly based on the correlation of the magnetic susceptibility with Core XK08-A1 dated using the OSL method (Fig. 2). The relationship between OSL ages and depth of Core XK08-A1 suggests that there are at least four sedimentary hiatuses in Lake Xingkai. Within dating errors, these occurred at 86.5 ± 11.2–65.5 ± 8.6, 53.3 ± 7.0–31.6 ± 4.1, 19 ± 2.5–8.2 ± 1.1, and 8.2 ± 1.1–0.4 ± 0.5 ka, respectively (Long et al., 2015). The upper 288 cm of sediments of Core XK08-A2 are well correlated with that of Core XK 08-A1 (Fig. 2). However, the OSL dating errors are relatively large for samples older than 55 ka, which may hinder assignment of the boundaries of MIS stages directly. It is worth noting that, during the last glacial-interglacial cycle, the sediment magnetic susceptibility of the cores shows low values during the warm periods (mid-Holocene and the last 0.4 ka) and high values during cold periods (MIS 4, early MIS 3, and MIS 2) . On the basis of this relationship, we further align the high magnetic susceptibility at 216–253 and 288–336 cm depth to MIS 5c and MIS 5e, respectively, and low magnetic susceptibility at 253–288 cm depth to MIS 5d (Table 1). In addition, a new AMS ^{14}C age on twigs at 64 cm depth of core XK08-A2 was dated to about 26.5 cal ka BP, which is consistent with the OSL age, further supporting that the OSL signals are fully bleached and the OSL dates are reliable (Long et al., 2015).

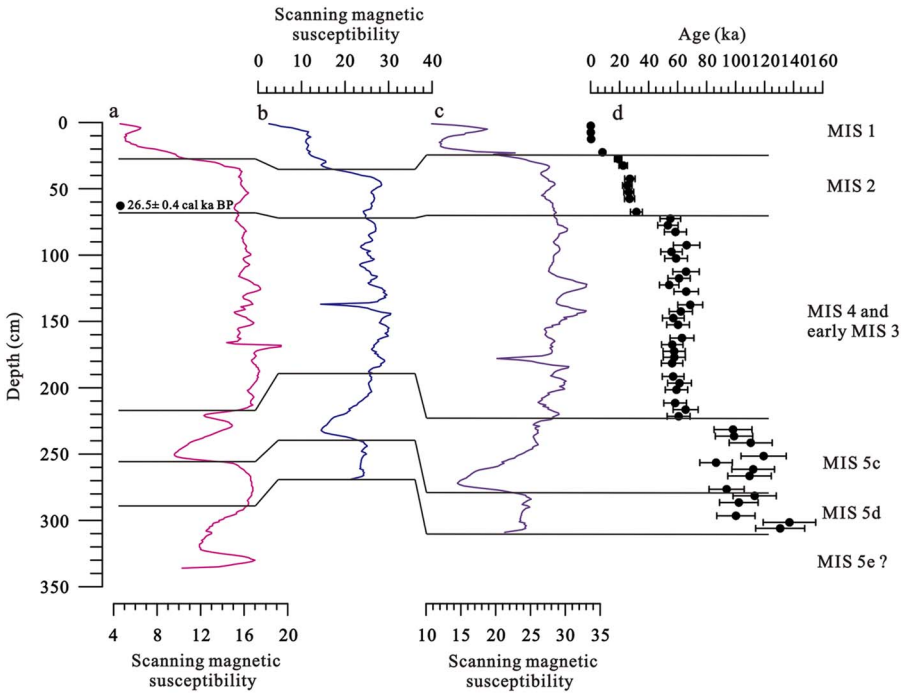

Figure 2. (color online) Correlation of (a) core XK08-A2 and(b) XK-1 with (c) the adjacent core XK08-A1, which was dated using the (d) optically stimulated luminescence method (Long et al., 2015).

https://doi.org/10.1017/qua.2017.81 Published online by Cambridge University Press

Table 1. Depth (cm) and the corresponding Marine Isotope Stage (MIS) of Lake Xingkai sediment cores.

XK08-A1	XK08–A2	XK-1	MIS
0–25	0–27	0–31	1
25–70	27–70	31–74	2
70–224	70–216	74–186	4 and early MIS 3
224–276	216–253	186–235	5c
276–308	253–288	235–269	5d
—	288–336	—	5e

Samples for grain-size analysis were taken from Core XK08-A2 at 1 cm intervals. The samples were first treated with 30% H_2O_2 at 75°C to remove organic matter, and then 10% HCl was added to remove carbonates and iron oxides. Subsequently, the samples were rinsed to neutral, and treated with 20 mL of 0.05 M $(NaPO_3)_6$ and dispersed using an ultrasonicator for 15 min. Grain-size distribution of the samples was measured using a Mastersizer 2000 laser grain-size analyzer ranging from 0.02 to 2000 μm and yielding 100 pairs of grain-size data. Every sample was measured three times and the mean was calculated and used for the analysis. The analytical error of the measurements is less than 1%. The median diameter (Md, the diameter at the 50th percentile of the distribution) and the percentages of clay (<2 μm), silt (2–63 μm), and sand (>63 μm) fractions of a sample were generated automatically. The original grain-size distributions of Core XK08-A2 were transferred into unmixed end members by BEMMA using a Markov Chain Monte Carlo algorithm (Yu et al., 2016). BEMMA is a hierarchical Bayesian model within the framework of Bayesian inference. To identify the number of end members, a birth-death process is used to browse the parameter space, while for the end member and fraction matrices, the Metropolis-Hastings-Green-within-Gibbs algorithm is used to deal with the move of the Markov chains and to update the model parameters and their hyperparameters (Yu et al., 2016). The end-member modeling was implemented in MATLAB R2012b.

RESULTS

The grain-size composition of lithic particles of Lake Xingkai sediments is shown in Figure 3a. The sediments are mainly composed of silt, with a content ranging from 61.9 to 93.8%, with a mean of 89.0%. The trend of the clay content is negatively correlated with that of silt, ranging from 5.1 to 19.8%, with a mean of 10.7%. The sand fraction is extremely low in Lake Xingkai sediments, but its content reaches as high as 33.0% at 254 cm deep. The Md values range from 5.0–15.6 μm, with a mean of 9.1 μm.

Representative grain-size distributions from Lake Xingkai sediments are shown in Figure 3b. The data are characterized by polymodal and asymmetrical forms. The first one is composed of two overlapping fine-grained particle populations with a modal size of 2 μm and 8 μm, respectively. The second popualtion is mainly composed of silt with a modal size of 10–20 μm and a small amount of fine-grained material. The third population is discontinuous, and shows a silt mode similar to the second type and an extremely coarse component with a modal size of 400–500 μm. However, this kind of distribution is rare and it only appears in several samples.

After a short burn-in period, the BEMMA model converges at three grain-size end members for Lake Xingkai sediments (Fig. 3c). The first end member (EM1) is characterized by a bimodal structure with a dominant mode at around 13 μm and a minor mode at around 2 μm. The fraction of EM1 ranges from 2.4 to 89.5%, with a mean of 19.3% (Fig. 3a). The second end member (EM2) is marked by an asymmetrical monomodal structure with a mode at around 10 μm. The fraction of EM2 ranges from 2.0 to 95.3%, with a mean of 60.0% (Fig. 3a). The third end member (EM3) also exhibits an asymmetrical monomodal structure, but with a dominant mode at around 5 μm. The fraction of EM3 ranges from 1.5 to 94.7%, with a mean of 20.7 % (Fig. 3a).

DISCUSSION

Interpretation of the grain-size end members

The grain-size composition of lacustrine sediments is influenced by sources and transport processes (Xiao et al., 1999; Xiao et al., 2009; Xiao et al., 2012; Xiao et al., 2013; Dietze et al., 2014). Determined by the geographic location and inflowing rivers, detrital particles in Lake Xingkai sediments would be expected to mainly be derived from materials transported by the rivers and streams during the rainy season and atmospheric dust deposits during the dry and windy spring season when the lake is covered by ice. To some extent, the unconsolidated sand near shorelines and reworked by the wind-driven waves could also contribute to the accumulation of clastic deposits in the lake.

Previous studies suggest that the two types of clastic sediments exhibit different fractions of mixing of specific grain-size components due to distinct transport dynamics. For example, fluvial sediments in northeast China are mainly composed of bed load sand with a dominant modal size of 100–400 μm and suspension fine silt with a dominant modal size of 10–15 μm (Xiao et al., 2012, 2013). However, the grain-size distribution of the fluvial component is also closely related to hydraulic conditions, so that the relative abundance would be highly modified by high and low hydrodynamics during the deposition process in the lake (Finney and Johnson, 1991). Generally, the sand component occurs only in the nearshore zone, where shallow water possesses high energy, and its relative abundance decreases significantly as water depth increases. The relative percentage of the fine silt component is considerably lower in the nearshore zone than the center of the lake (Xiao et al., 2013). In Lake Xingkai, EM1 and EM2, with a dominant modal size of 13 and 10 μm, respectively, are consistent with the modal size of fluvial source. This suggests that EM1 and

https://doi.org/10.1017/qua.2017.81 Published online by Cambridge University Press

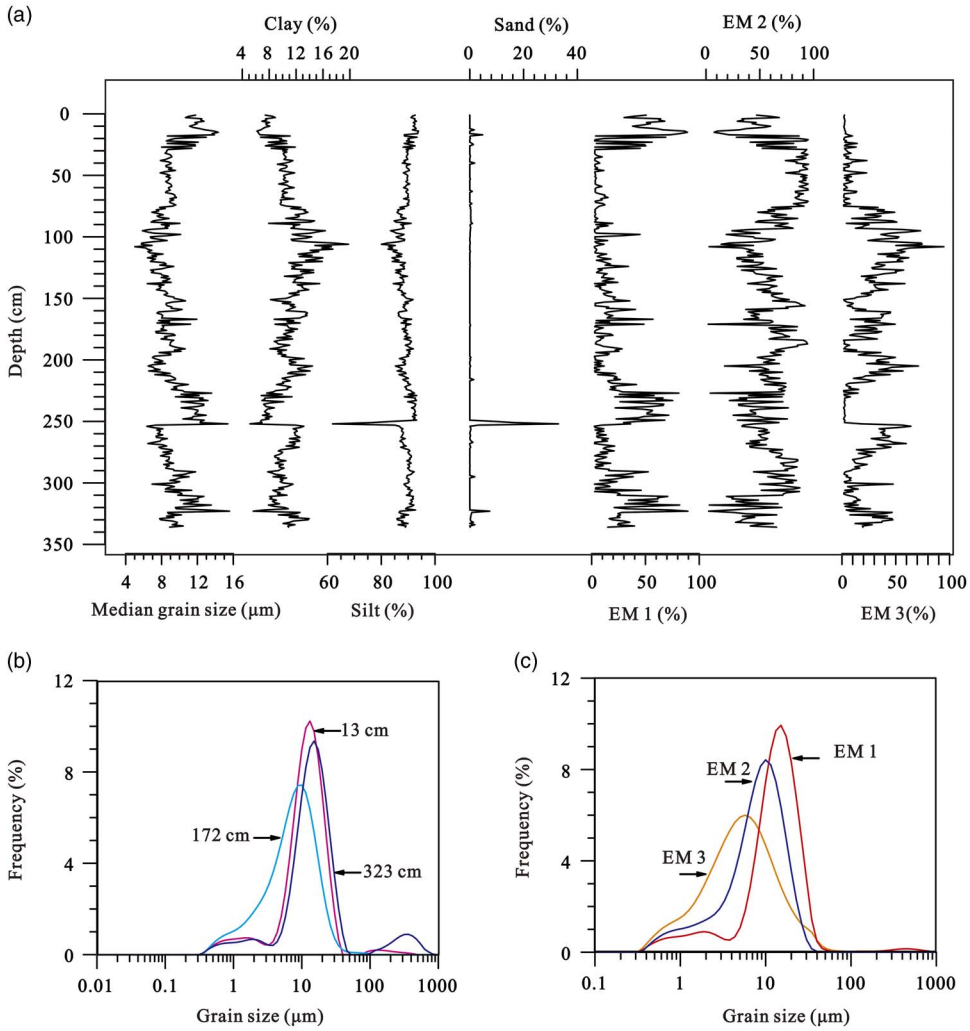

Figure 3. (color online) Results of grain-size analysis of core XK08-A2. (a) Variations in the median grain size, fraction of clay, silt, and sand, as well as the fraction of each EM 1-3 output from BEMMA. (b) Grain-size distributions of representative samples. (c) Grain-size distribution of EM 1-3 obtained from BEMMA.

EM2 were transported by the riverine inflows and can be used as proxies for the hydraulic dynamics of Lake Xingkai. Lake level variation history could also be reconstructed through beach ridges (Thomas et al., 2009; Rades et al., 2013). Based on the characteristics of the grain-size distribution, the ridges around Lake Xingkai are aeolian, not wave-built or lacustrine sedimentary formations, and the age of the ridges can be used as an indicator of regressional periods (Zhu et al., 2011; Long and Shen, 2017). New ages for the sandy ridges around Lake Xingkai suggests that a distinct period of lake lowstand occurred at ~32–15 ka (Long and Shen, 2017). However, the sediments from this period are dominated by EM2 and characterized by fine silt. Therefore, considering the absence of the nearshore sedimentary characteristics, the variation of lake level would not influence the hydraulic dynamics significantly at the coring location since the last interglaciation.

Increased precipitation could enhance the transport capacity of rivers and streams, leading to a coarser grain size in the center of the lake (Chen et al., 2004). Thus, the modal size of the fine silt component may reflect precipitation intensity in the watershed of the lake: a higher percentage of the silt-size fraction and an increase in the grain size would reflect intensified precipitation rates (Peng et al., 2005). Because the precipitation at Lake Xingkai is mainly determined by the EASM, we infer that EM1 was transported to the lake by rivers and streams during heavy rainfall influenced by the intensified EASM, while EM2 was transported to the lake by meltwater in spring or during rainfall when the EASM retreated from the lake region. Assuming a similar content of suspended particles in the inflows, we interpret the ratio of EM1 to the sum of EM1 and EM2 fractions of Lake Xingkai sediments as a proxy index for past changes in the EASM intensity. Specifically, the higher the EM1 / (EM1 + EM2) ratio, the stronger the EASM and thus the summer precipitation in the lake region.

Modern observations and lacustrine varve characteristics suggest that atmospheric dust is also an important component of lacustrine sediments in middle latitudes of the northern Hemisphere (Liu et al., 2009; Xiao et al., 2012; Chen et al., 2013; Xiao et al., 2013; Dietze et al., 2014). The particle size

https://doi.org/10.1017/qua.2017.81 Published online by Cambridge University Press

distribution of EM3 is similar to dust samples collected from recent dust events; for example, the 2002 dust storm in the Longgang area and the 2011 wet deposited dust in Harbin in northeastern China (Fig. 4a; Chu et al., 2009; Xie et al., 2015). EM3 is also similar to the grain-size distribution of the fine component of the Chinese loess-paleosol deposits, aeolian sediments in Cheju Island, Korea, and North Pacific deep-sea sediments (Fig. 4b–d; Rea and Hovan, 1995; Lim and Matsumoto, 2006; Sun, 2004; Serno et al., 2014). These lines of evidence suggest that EM3 in Lake Xingkai sediments represents an aeolian dust origin. However, different grain-size fractions have been used to trace the dust deposits in lake sediment, such as sand fraction of 56–282.5 μm in Lake Sugan in the Qaidam Basin and fine silt (<10 μm) quartz particles in Lake Biwa in central Japan (Xiao et al., 1999; Chen et al., 2013). This difference may be attributed to different sorting mechanisms during wind transport and deposition processes. Theoretically, particles larger than 70 μm would retained in the aeolian source area; the fraction with average grain size 10–70 μm is transported by surface winds to a distance about 250 km; and the fine component (average grain size of < 10 μm) is mainly transported by upper-level air flow in long-term suspension (Tsoar and Pye, 1987; Sun et al., 2008). Therefore, lakes near the dust source area would receive more of the sand fraction, while lakes in humid area are mainly influenced by fine dust. In addition, the surfaces of sandy ridges around the lake are covered by vegetation in summer and freeze from winter to spring, the near shoreline materials that could be transported by wind to the center of the lake would be limited. Lake Xingkai is blocked by Changbai Mountains and distant from the arid and semiarid zones in north China and the Mongolian Gobi in the west, thus, the fine silt component EM3 seems to be very sensitive and strongly related to dust activity, and this fraction can be used to indicate that the dust is derived from Mongolia and the northeastern Chinese sand areas.

Evolution of the East Asian summer monsoon

Aspects of the history of the EASM evolution since 130 ka BP can be inferred from the proxy defined as EM1 / (EM1 + EM2)

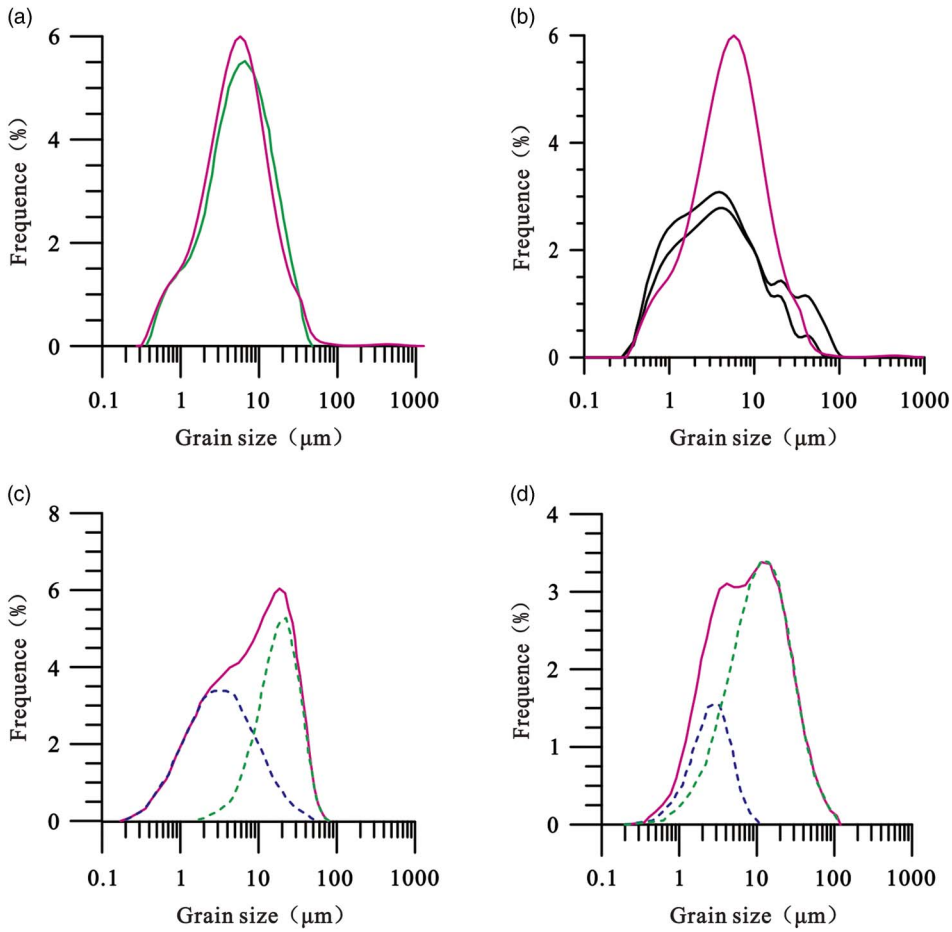

Figure 4. (color online) Comparison of the grain-size distribution of EM3 with that of aeolian dust elsewhere. (a) Wet-deposition dust in Harbin, NE China (green line; Xie et al., 2015). (b) Westerly-delivered dust in North Pacific Ocean (black lines; Serno et al., 2014). (c) Loess from the Chinese Loess Plateau (red line; Sun et al., 2002). (d) Aeolian quartz in Cheju Island, Korea (red line; Lim and Matsumoto 2006). The dashed lines in (c) and (d) represent the fine and coarse components obtained by fitting using the Weibull distribution function. (For interpretation of the references to color inn this figure legend, the reader is referred to the web version of this article.)

https://doi.org/10.1017/qua.2017.81 Published online by Cambridge University Press

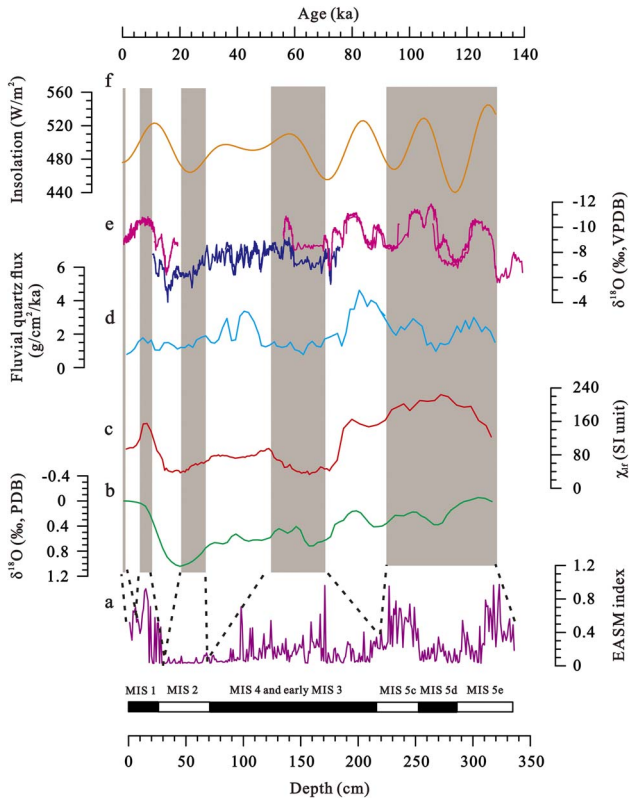

Figure 5. (color online) Comparison of the EASM index derived from core XK08-A2 grain size end members (a) with other climate records. (b) Reconstructed mean ocean water $\delta^{18}O$ (Waelbroeck et al., 2002). (c) Magnetic susceptibility from Luochuan in Chinese Loess Plateau (An et al., 1991). (d) Fluvial quartz flux from Lake Biwa Japan (Xiao et al., 1999). (e) $\delta^{18}O$ records of stalagmite from Sanbao and Hulu Cave in east China (Wang et al., 2001, 2008). (f) June insolation at 60°N (Berger and Loutre, 1991). Shaded intervals denote possible intervals during which EASM was reconstructed by Core XK08-A2.

from Lake Xingkai (Fig. 5a). The moisture history can be divided into three stages: (1) a generally strong EASM interval during MIS 5 with a phase of weak EASM corresponding to MIS 5d; (2) an interval of weakening EASM from MIS 4 to MIS 2; and (3) a moist period during MIS 1. Pollen data from core XK-1 revealed a similar moisture history. For example, the rapid increase in tree pollen percentages from MIS 5d to 5c suggests that the climate became warm and humid; from MIS 4 to MIS 2, the forest in the adjacent mountains retreated and local vegetation was replaced by Chenopodiaceae-dominated steppe, indicating that the climate become cold and dry; the highest pollen percentages of thermophilous *Quercus*, *Pinus,* and *Ulmus* indicate a relatively strong EASM during MIS 1 (Wu and Shen, 2010a). The pattern of changes in the EASM during the last glacial-interglacial cycle is consistent with other records from the EASM region. During the last interglaciation and the Holocene, for instance, high magnetic susceptibility values suggest intensified pedogenesis in the Chinese Loess Plateau (Fig. 5c; An et al., 1991); high fluvial quartz fluxes indicate an increased amount of clastic material entering the Lake Biwa in Japan from the catchments (Fig. 5d; Xiao et al., 1999); paleo-shorelines dated by OSL show high lake levels occurring in northwestern China (Long et al., 2012; Lai et al., 2014; Li et al., 2015); and the lower oxygen isotope values of cave carbonates in central China suggest increased summer monsoon precipitation (Fig. 5e; Wang et al., 2001, 2008). During the last glaciation, pedogenesis in the Chinese Loess Plateau was weakened, the amount of clastic materials entering Lake Biwa from the surrounding areas decreased, lakes in northwestern China were at very low levels, and a decrease in summer monsoon precipitation is also indicated by high oxygen isotope values from cave carbonates in central China (An et al., 1991; Xiao et al., 1999; Wang et al., 2001, 2008; Long et al., 2012; Lai et al., 2014; Li et al., 2015). Furthermore, there are numerous short-term abrupt changes superimposed on the long-term trend of EASM intensity. Within the dating error, the oscillations also correspond to the reported intervals of abrupt EASM fluctuations since the last interglaciation inferred from the records of speleothems and loess-paleosol profiles in China (Porter and An, 1995; Wang et al., 2001, 2008; Sun et al., 2012).

Despite these changes inferred from fluvial processes, the sedimentary hiatuses of Lake Xingkai are in large part related to climate change. With weakened summer monsoon intensity, lakes in the monsoon region were characterized by low levels, which could trigger deflation and result in the formation of hiatuses in the sedimentary sequence (Jones et al., 2012). For Lake Xingkai, sedimentary hiatuses occurred at 8.2 ± 1.1–0.4 ± 0.5 ka and may be caused by the low lake level during the period 1.2–0.5 ka, which corresponds to the age of the sandy ridges (Long and Shen, 2017). The extreme droughts could have led to scouring of the lakebed and the renewal of lake sediment accumulation indicates the termination of the dry events. We therefore also infer that other sedimentary hiatuses of Lake Xingkai, which occurred at 86.5 ± 11.2–65.5 ± 8.6, 53.3 ± 7.0–31.6 ± 4.1, 19 ± 2.5–8.2 ± 1.1 ka, are possibly related to the significant weakening of the EASM during Heinrich events 6, 3, and 1 and the Younger Dryas, within dating uncertainties (Wang et al., 2001).

On the orbital scale, the grain-size record of the EASM from Lake Xingkai can be compared with summer insolation in the Northern Hemisphere during this interval (Fig. 5f; Berger and Loutre, 1991). In the study region, most of the annual precipitation falls in the summer when the monsoonal rain belt migrates to its northern limit. The increased solar insolation during the interglaciation would increase the sea-surface temperature of the west Pacific warm pool, and thus enhance the atmospheric pressure gradient between the ocean and the Eurasian continent, which, in turn, would intensify the penetration of the moist maritime airmasses into the interior of the continent. However, not only did solar insolation decrease during the glaciations, but the ice sheets in the high latitudes of the Northern Hemisphere also expanded (Fig. 5b; Waelbroeck et al., 2002). During cold periods, the Arctic polar front and the westerlies moved southward as the ice sheets expanded, which would deflect the Intertropical

https://doi.org/10.1017/qua.2017.81 Published online by Cambridge University Press

Convergence Zone southward, leading to an anti-phased relationship between the EASM and the westerlies in the middle latitudes (An et al., 2012). This interplay between the high- and low-latitude climate variability controls the hydroclimate regime in the middle latitudes of the Northern Hemisphere on orbital time scales.

Changes in the background atmospheric dust loading

As shown in Figure 6, the relative content of dust in the atmosphere from the last interglacial stage can be inferred using the changes in the fine fraction EM3 of Lake Xingkai sediments. The proxy indicates that dust was primarily deposited during the MIS 5d and from MIS 4 to early MIS 3. In contrast, dust loading in the atmosphere was generally low during MIS 2 and MIS 5e, 5c, and MIS 1. The generally higher atmospheric dust loadings from MIS 4 to early MIS 3 are consistent with the variation in sediment rate of loess-paleosol profiles in northeast China, the Chinese Loess Plateau, and northwest China based on high-resolution OSL chronology (Fig. 6d and f; Sun and An, 2005; Yi et al., 2015; Li et al., 2016), relatively high aeolian quartz flux in Lake Biwa in central Japan (Fig. 6e; Xiao et al., 1999), and high dust influx as recorded in marine sediments of the North Pacific (Rea and Hovan, 1995). During the weakened EASM period, decreased precipitation would significantly lower soil moisture and reduce vegetation cover on in the Asian arid areas, leading to higher rates of soil erosion (Fig. 6b). Meanwhile, many large lakes in northwestern China formed during the previous interglaciation dried, and deserts expanded in north China (Long et al., 2012; Lu et al., 2013; Lai et al., 2014; Li et al., 2015), providing abundant fine silt and increasing dust emissions (Yang et al., 2008). In addition, the East Asian winter monsoon was greatly strengthened as indicated by the grain size of aeolian sediments in the Chinese Loess Plateau (Sun et al., 2012). Therefore, large dust source areas and strong winter monsoon promoted the emission of dust, resulting in more dust deposition in the middle latitudes during cold periods.

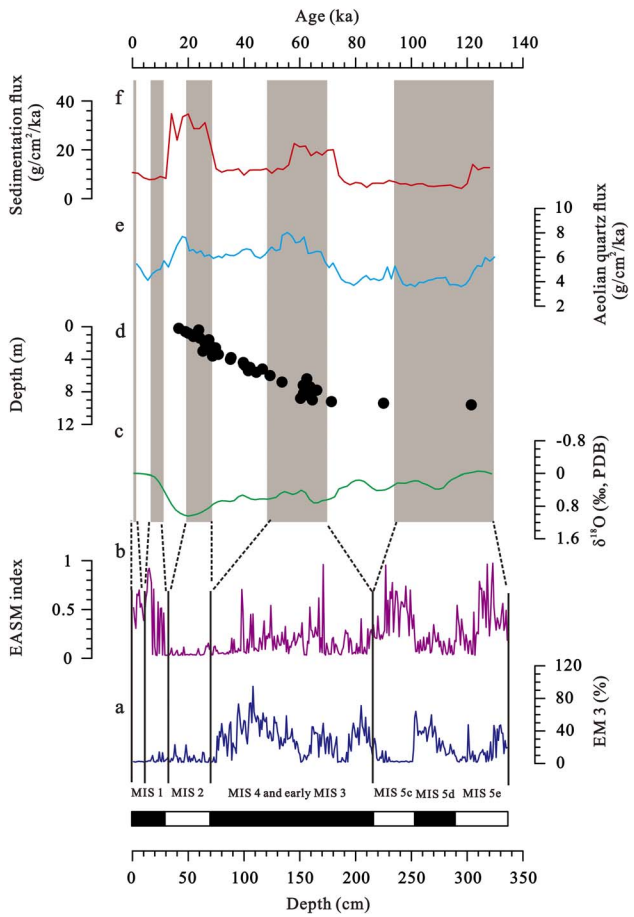

Figure 6. (color online) Comparison of the variations in atmospheric dust loading (a) with other regional conditions. (b) EASM index from Lake Xingkai (this study). (c) Reconstructed mean ocean water $\delta^{18}O$ (Waelbroeck et al., 2002). (d) Accumulation rate of Sanbahuo loess-paleosol profile in northeast China (Yi et al., 2015). (e) Aeolian quartz flux from Lake Biwa, Japan (Xiao et al., 1999). (f) Sediment flux of Lingtai loess-paleosol profile from the central Chinese Loess Plateau (Sun and An, 2005). Shaded intervals indicate possible intervals during which paleoenvironmental information was revealed by Core XK08-A2.

The EASM was weak and the resultant Asian dust source conditions were more favorable for dust emission during MIS 2. However, reduced vegetation cover under the weakened monsoonal circulation could not fully account for the inconsistent results of Lake Xingkai. In the Northern Hemisphere middle latitudes, the high-altitude westerlies were suggested to be the major carrier of fine dust (Nagashima et al., 2007; Kang et al., 2015). Nowadays, blocked by the Qinghai-Tibetan Plateau, the axis of the high-altitude westerlies is located to the south of the Himalayas from December to April, and then it moves to the northern margin of the Qinghai-Tibetan Plateau in early summer (Schiemann et al., 2009). During the glacials, the southward migration of the mean position of the westerlies could affect the provenance and transport of aeolian dust in downwind of the Asian dust source areas (Nagashima et al., 2007; Kang et al., 2015). As the mean position of the axis of the westerlies is closely related to the Northern Hemispheric ice volume, the annually averaged westerlies axis during MIS 2 should be deflected southward when compared with that during MIS 5d, MIS 4, and early MIS 3 (Fig. 6c; Kitoh et al., 2001; Waelbroeck et al., 2002). Therefore, it is reasonable to infer that there may have a lack of effective westerlies over Lake Xingkai during MIS 2, so the dust was mainly deposited in the Chinese Loess Plateau and the North Pacific between 35°N and 40°N. In contrast, during MIS 5d, MIS 4, and early MIS 3, the relative northward migration of the westerlies over the Mongolia Gobi and northeast China may have delivered a large amount of dust to Lake Xingkai.

CONCLUSIONS

The grain-size end-member unmixing program, BEMMA, was used to partition the polymodal grain-size distributions

https://doi.org/10.1017/qua.2017.81 Published online by Cambridge University Press

of Lake Xingkai sediments since the last interglaciation. The results suggest that the lacustrine deposits contain three overlapping end members with a modal size of 13, 10, and 5 μm, respectively. EM1 and EM2 are related to fluvial processes and the ratio of EM1 / (EM1 + EM2) was sensitive to the variation of local hydroclimatic conditions, which are closely related to the EASM variations. The coherence between the EASM evolution and Northern Hemispheric insolation since the last interglaciation indicates that solar insolation may have regulated the hydroclimatic change in northeast Asia. EM3 is derived from atmospheric dust loading, and it reflects the background dust input to the lake. High atmospheric dust concentration in this area generally occurred in MIS 5d, MIS 4, and early MIS 3, when the climate was dry in the Asian dust source region. Low dust input prevailed in this area during MIS 2, due to the southward displacement of the westerlies driven by maximum ice-sheet expansion in the high latitudes. Our results suggest that the BEMMA method represents a powerful tool for the unmixing of the polymodal grain-size distributions of lacustrine sediments, which, in turn, deepens our understanding of the sedimentary processes of clastic materials in lake systems and the environmental conditions of the catchment during the geological past.

ACKNOWLEDGMENTS

We would like to express our gratitude to the editor and two anonymous reviewers for helpful comments that improved the quality of this manuscript. We also want to thank Dr. Yong Wang for field assistance and Dr. Jie Chang for correcting the English language. This research was supported by the National Natural Science Foundation of China (Grant Nos. 41430530 and 41621002) and the international partnership program for creative research teams of the Chinese Academy of sciences (No. KZZD-EW-TZ-08).

REFERENCES

An, Z., Colman, S.M., Zhou, W., Li, X., Brown, E.T., Jull, A.J.T., Cai, Y., et al., 2012. Interplay between the Westerlies and Asian monsoon recorded in Lake Qinghai sediments since 32 ka. *Scientific Reports* 2: A619. http://dx.doi.org/10.1038/srep00619.

An, Z., Kukla, G.J., Porter, S.C., Xiao, J., 1991. Magnetic susceptibility evidence of monsoon variation on the Loess Plateau of central China during the last 130,000 years. *Quaternary Research* 36, 29–36.

Berger, A., Loutre, M.-F., 1991. Insolation values for the climate of the last 10 million years. *Quaternary Science Reviews* 10, 297–317.

Chen, F., Qiang, M., Zhou, A., Xiao, S., Chen, J., Sun, D., 2013. A 2000-year dust storm record from Lake Sugan in the dust source area of arid China. *Journal of Geophysical Research: Atmospheres* 118, 2149–2160.

Chen, J.A., Wan, G., Zhang, D., Zhang, F., Huang, R., 2004. Environmental records of lacustrine sediments in different time scales: sediment grain size as an example. *Science in China Series D: Earth Sciences* 47, 954–960.

Chu, G., Sun, Q., Zhaoyan, G., Rioual, P., Qiang, L., Kaijun, W., Han, J., Liu, J., 2009. Dust records from varved lacustrine sediments of two neighboring lakes in northeastern China over the last 1400 years. *Quaternary International* 194, 108–118.

Dietze, E., Hartmann, K., Diekmann, B., Ijmker, J., Lehmkuhl, F., Opitz, S., Stauch, G., Wünnemann, B., Borchers, A., 2012. An end-member algorithm for deciphering modern detrital processes from lake sediments of Lake Donggi Cona, NE Tibetan Plateau, China. *Sedimentary Geology* 243–244, 169–180.

Dietze, E., Maussion, F., Ahlborn, M., Diekmann, B., Hartmann, K., Henkel, K., Kasper, T., Lockot, G., Opitz, S., Haberzettl, T., 2014. Sediment transport processes across the Tibetan Plateau inferred from robust grain-size end members in lake sediments. *Climate of the Past* 10, 91–106.

Finney, B.P., Johnson, T.C., 1991. Sedimentation in Lake Malawi (East Africa) during the past 10,000 years: a continuous paleoclimatic record from the southern tropics. *Palaeogeography, Palaeoclimatology, Palaeoecology* 85, 351–366.

Jones, R.T., Cook, C.G., Zhang, E., Langdon, P.G., Jordan, J., Turney, C., 2012. Holocene environmental change at Lake Shudu, Yunnan Province, southwestern China. *Hydrobiologia* 693, 223–235.

Kang, S., Roberts, H.M., Wang, X., An, Z., Wang, M., 2015. Mass accumulation rate changes in Chinese loess during MIS 2, and asynchrony with records from Greenland ice cores and North Pacific Ocean sediments during the Last Glacial Maximum. *Aeolian Research* 19, Part B. 251–258.

Kitoh, A., Murakami, S., Koide, H., 2001. A simulation of the Last Glacial Maximum with a coupled atmosphere-ocean GCM. *Geophysical Research Letters* 28, 2221–2224.

Lai, Z., Mischke, S., Madsen, D., 2014. Paleoenvironmental implications of new OSL dates on the formation of the "Shell Bar" in the Qaidam Basin, northeastern Qinghai-Tibetan Plateau. *Journal of Paleolimnology* 51, 197–210.

Li, G., Jin, M., Duan, Y., Madsen, D.B., Li, F., Yang, L., Wei, H., Chen, F., 2015. Quartz and K-feldspar luminescence dating of a Marine Isotope Stage 5 megalake in the Juyanze Basin, central Gobi Desert, China. *Palaeogeography, Palaeoclimatology, Palaeoecology* 440, 96–109.

Li, G., Rao, Z., Duan, Y., Xia, D., Wang, L., Madsen, D.B., Jia, J., Wei, H., Qiang, M., Chen, J., Chen, F., 2016. Paleoenvironmental changes recorded in a luminescence dated loess/paleosol sequence from the Tianshan Mountains, arid central Asia, since the Penultimate Glaciation. *Earth and Planetary Science Letters* 448, 1–12.

Lim, J., Matsumoto, E., 2006. Bimodal grain-size distribution of aeolian quartz in a maar of Cheju Island, Korea, during the last 6500 years: its flux variation and controlling factor. *Geophysical Research Letters* 33, L21816. http://dx.doi.org/10.1029/2006GL027432.

Liu, X., Dong, H., Yang, X., Herzschuh, U., Zhang, E., Stuut, J.-B.W., Wang, Y., 2009. Late Holocene forcing of the Asian winter and summer monsoon as evidenced by proxy records from the northern Qinghai–Tibetan Plateau. *Earth and Planetary Science Letters* 280, 276–284.

Long, H., Lai, Z., Fuchs, M., Zhang, J., Li, Y., 2012. Timing of Late Quaternary palaeolake evolution in Tengger Desert of northern China and its possible forcing mechanisms. *Global and Planetary Change* 92–93, 119–129.

Long, H., Shen, J., 2017. Sandy beach ridges from Xingkai Lake (NE Asia): Timing and response to palaeoclimate. *Quaternary International* 430 (B), 21–31.

Long, H., Shen, J., Wang, Y., Gao, L., Frechen, M., 2015. High-resolution OSL dating of a late Quaternary sequence from Xingkai Lake (NE Asia): chronological challenge of the "MIS 3a

Mega-paleolake" hypothesis in China. *Earth and Planetary Science Letters* 428, 281–292.

Lu, H., Yi, S., Xu, Z., Zhou, Y., Zeng, L., Zhu, F., Feng, H., et al., 2013. Chinese deserts and sand fields in Last Glacial Maximum and Holocene Optimum. *Chinese Science Bulletin* 58, 2775–2783.

Maher, B.A., Prospero, J.M., Mackie, D., Gaiero, D., Hesse, P.P., Balkanski, Y., 2010. Global connections between aeolian dust, climate and ocean biogeochemistry at the present day and at the last glacial maximum. *Earth-Science Reviews* 99, 61–97.

Middleton, N.J., Sternberg, T., 2013. Climate hazards in drylands: a review. *Earth-Science Reviews* 126, 48–57.

Nagashima, K., Tada, R., Matsui, H., Irino, T., Tani, A., Toyoda, S., 2007. Orbital- and millennial-scale variations in Asian dust transport path to the Japan Sea. *Palaeogeography, Palaeoclimatology, Palaeoecology* 247, 144–161.

Peng, Y., Xiao, J., Nakamura, T., Liu, B., Inouchi, Y., 2005. Holocene East Asian monsoonal precipitation pattern revealed by grain-size distribution of core sediments of Daihai Lake in Inner Mongolia of north-central China. *Earth and Planetary Science Letters* 233, 467–479.

Pigati, J.S., Quade, J., Wilson, J., Jull, A.J.T., Lifton, N.A., 2007. Development of low-background vacuum extraction and graphitization systems for 14C dating of old (40–60 ka) samples. *Quaternary International* 166, 4–14.

Porter, S.C., An, Z., 1995. Correlation between climate events in the North-Atlantic and China during last glaciation. *Nature* 375, 305–308.

Rades, E.F., Hetzel, R., Xu, Q., Ding, L., 2013. Constraining Holocene lake-level highstands on the Tibetan plateau by 10Be exposure dating: a case study at Tangra Yumco, southern Tibet. *Quaternary Science Reviews* 82, 68–77.

Rea, D.K., Hovan, S.A., 1995. Grain size distribution and depositional processes of the mineral component of abyssal sediments: Lessons from the North Pacific. *Paleoceanography* 10, 251–258.

Schiemann, R., Lüthi, D., Schär, C., 2009. Seasonality and interannual variability of the westerly jet in the Tibetan Plateau region. *Journal of Climate* 22, 2940–2957.

Serno, S., Winckler, G., Anderson, R.F., Hayes, C.T., McGee, D., Machalett, B., Ren, H., Straub, S.M., Gersonde, R., Haug, G.H., 2014. Eolian dust input to the Subarctic North Pacific. *Earth and Planetary Science Letters* 387, 252–263.

Shen, J., 2013. Spatiotemporal variations of Chinese lakes and their driving mechanisms since the Last Glacial Maximum: a review and synthesis of lacustrine sediment archives. *Chinese Science Bulletin* 58, 17–31.

Steffensen, J.P., 1997. The size distribution of microparticles from selected segments of the Greenland Ice Core Project ice core representing different climatic periods. *Journal of Geophysical Research: Oceans* 102, 26755–26763.

Sun, D., 2004. Monsoon and westerly circulation changes recorded in the late Cenozoic aeolian sequences of Northern China. *Global and Planetary Change* 41, 63–80.

Sun, D., Bloemendal, J., Rea, D.K., Vandenberghe, J., Jiang, F., An, Z., Su, R., 2002. Grain-size distribution function of polymodal sediments in hydraulic and aeolian environments, and numerical partitioning of the sedimentary components. *Sedimentary Geology* 152, 263–277.

Sun, D., Su, R., Bloemendal, J., Lu, H., 2008. Grain-size and accumulation rate records from Late Cenozoic aeolian sequences in northern China: implications for variations in the East Asian winter monsoon and westerly atmospheric circulation. *Palaeogeography, Palaeoclimatology, Palaeoecology* 264, 39–53.

Sun, Y., An, Z., 2005. Late Pliocene-Pleistocene changes in mass accumulation rates of eolian deposits on the central Chinese Loess Plateau. *Journal of Geophysical Research: Atmospheres* 110, D23101. http://dx.doi.org/10.1029/2005JD006064.

Sun, Y., Clemens, S.C., Morrill, C., Lin, X., Wang, X., An, Z., 2012. Influence of Atlantic meridional overturning circulation on the East Asian winter monsoon. *Nature Geoscience* 5, 46–49.

Thomas, D.S.G., Bailey, R., Shaw, P.A., Durcan, J.A., Singarayer, J.S., 2009. Late Quaternary highstands at Lake Chilwa, Malawi: frequency, timing and possible forcing mechanisms in the last 44 ka. *Quaternary Science Reviews* 28, 526–539.

Tsoar, H., Pye, K., 1987. Dust transport and the question of desert loess formation. *Sedimentology* 34, 139–153.

Uno, I., Eguchi, K., Yumimoto, K., Takemura, T., Shimizu, A., Uematsu, M., Liu, Z., Wang, Z., Hara, Y., Sugimoto, N., 2009. Asian dust transported one full circuit around the globe. *Nature Geoscience* 2, 557–560.

Waelbroeck, C., Labeyrie, L., Michel, E., Duplessy, J.C., McManus, J.F., Lambeck, K., Balbon, E., Labracherie, M., 2002. Sea-level and deep water temperature changes derived from benthic foraminifera isotopic records. *Quaternary Science Reviews* 21, 295–305.

Wan, B., Zhong, Y., 1997. Features analysis and divisions of new tectonic movement in northeast China. [In Chinese.] *Seismological Research of Northeast China* 13, 64–75.

Wang, P.X., Wang, B., Cheng, H., Fasullo, J., Guo, Z.T., Kiefer, T., Liu, Z.Y., 2014. The global monsoon across timescales: coherent variability of regional monsoons. *Climate of the Past* 10, 2007–2052.

Wang, Y., Cheng, H., Edwards, R.L., Kong, X., Shao, X., Chen, S., Wu, J., Jiang, X., Wang, X., An, Z., 2008. Millennial- and orbital-scale changes in the East Asian monsoon over the past 224,000 years. *Nature* 451, 1090–1093.

Wang, Y.J., Cheng, H., Edwards, R.L., An, Z.S., Wu, J.Y., Shen, C.-C., Dorale, J.A., 2001. A high-resolution absolute-dated late Pleistocene monsoon record from Hulu Cave, China. *Science* 294, 2345–2348.

Williams, D.F., Kuzmin, M.I., Prokopenko, A.A., Karabanov, E.B., Khursevich, G.K., Bezrukova, E.V., 2001. The Lake Baikal drilling project in the context of a global lake drilling initiative. *Quaternary International* 80–81, 3–18.

Wu, J., Shen, J., 2009. Paleoenvironmental and paleoclimatic changes reflected by diffuse reflectance spectroscopy and magnetic susceptibility from Xingkai Lake sediments. [In Chinese.] Marine. *Geology and Quaternary Geology* 29, 123–131.

Wu, J., Shen, J., 2010a. Paleoclimate evolution since 27.7 ka BP reflected by grain size variation of a sediment core from Lake Xingkai, northeastern Asia. [In Chinese.] *Journal of Lake Science* 22, 110–118.

Wu, J., Shen, J., 2010b. Paleoenvironmental and paleoclimatic changes in Lake Xingkai inferred from stable carbon and nitrogen isotopes of bulk organic matter since 28 ka BP. [In Chinese.] *Acta Sedimentologica Sinica* 28, 365–372.

Xiao, J., Chang, Z., Fan, J., Zhou, L., Zhai, D., Wen, R., Qin, X., 2012. The link between grain-size components and depositional processes in a modern clastic lake. *Sedimentology* 59, 1050–1062.

Xiao, J., Chang, Z., Si, B., Qin, X., Itoh, S., Lomtatidze, Z., 2009. Partitioning of the grain-size components of Dali Lake core

https://doi.org/10.1017/qua.2017.81 Published online by Cambridge University Press

sediments: evidence for lake-level changes during the Holocene. *Journal of Paleolimnology* 42, 249–260.

Xiao, J., Fan, J., Zhou, L., Zhai, D., Wen, R., Qin, X., 2013. A model for linking grain-size component to lake level status of a modern clastic lake. *Journal of Asian Earth Sciences* 69, 149–158.

Xiao, J., Si, B., Zhai, D., Itoh, S., Lomtatidze, Z., 2008. Hydrology of Dali Lake in central-eastern Inner Mongolia and Holocene East Asian monsoon variability. *Journal of Paleolimnology* 40, 519–528.

Xiao, J.L., An, Z.S., Liu, T.S., Inouchi, Y., Kumai, H., Yoshikawa, S., Kondo, Y., 1999. East Asian monsoon variation during the last 130,000 Years: evidence from the Loess Plateau of central China and Lake Biwa of Japan. *Quaternary Science Reviews* 18, 147–157.

Xie, Y., Chi, Y., Meng, J., Guo, L., Wang, Y., 2015. Grain-size and Sr–Nd isotopic compositions of dry- and wet-deposited dusts during the same dust-storm event in Harbin, China: implications for source, transport–deposition modes, dynamic mechanism and formation of aeolian loess. *Environmental Earth Sciences* 74, 6489–6502.

Yang, L.-R., Yue, L.-P., Li, Z.-P., 2008. The influence of dry lakebeds, degraded sandy grasslands and abandoned farmland in the arid inlands of northern China on the grain size distribution of East Asian aeolian dust. *Environmental Geology* 53, 1767–1775.

Yi, S., Buylaert, J.-P., Murray, A.S., Thiel, C., Zeng, L., Lu, H., 2015. High resolution OSL and post-IR IRSL dating of the last interglacial–glacial cycle at the Sanbahuo loess site (northeastern China). *Quaternary Geochronology* 30, Part B. 200–206.

Yin, J., Fang, X., Su, Y., 2016. Correlation between climate and grain harvest fluctuations and the dynastic transitions and prosperity in China over the past two millennia. *The Holocene* 26, 1914–1923.

Yu, S.-Y., Colman, S.M., Li, L., 2016. BEMMA: A hierarchical Bayesian end-member modeling analysis of sediment grain-size distributions. *Mathematical Geosciences* 48, 723–741.

Zhu, Y., Shen, J., Lei, G., Wang, Y., 2011. Environmental evolution of Xingkai (Khanka) Lake since 200 ka by OSL dating of sand hills. *Chinese Science Bulletin* 56, 2604–2612.

https://doi.org/10.1017/qua.2017.81 Published online by Cambridge University Press